MethodsX 13 (2024) 103073

Contents lists available at ScienceDirect

MethodsX

journal homepage: www.elsevier.com/locate/methodsx

Methodology for the correction of a CBCT volume from the skull to the natural head position ☆,☆☆

Carlos Andrés Ferro Sánchez [a,*], Cristian Orlando Diaz Laverde [b], Sandra Esperanza Nope Rodríguez [c], Gilber Alexis Corrales Gallego [a], Juan Fernando Aristizábal [b], Oscar Iván Campo Salazar [a]

[a] Faculty of Engineering, Universidad Autónoma de Occidente, Cali, Colombia
[b] Health Faculty, Universidad del Valle, Cali, Colombia
[c] Escuela de Ingeniería Eléctrica y Electrónica (EIEE), Facultad de Ingeniería, Universidad del Valle, Colombia

ARTICLE INFO

Method name:
Method for Correcting Natural Head Position in CBCT Volumes Using RAI Orientation, YOLOv8, and VGG19 (M-CNHP-RYV): A Sella-Nasion-Based Approach (SN-CM-NHP)

Keywords:
NHP
Natural head position
CBCT
Deep learning
Segmentation
Cephalometric

ABSTRACT

The orientation of the head during the acquisition of cone beam computed tomography (CBCT) is crucial for accurate cephalometric measurements. However, involuntary head movements during the scan can result in misaligned images. This study presents a method to correct the natural head position (NHP) in CBCT skull images after acquisition. Initially, slices were reorganized, and volumes were oriented in RAI coordinates. Next, the Yaw angle in the axial plane was estimated using the fronto-zygomatic sutures (FZS). The Roll angle in the coronal plane was estimated using the centroids of the ocular cavities. Finally, the Pitch angle in the sagittal plane was measured (by the Sella Turcica (S) and Nasion (N) as reference points) and adjusted to reference values of 3.8° for males and 4.1° for females. These calculated angles are used to adjust the CBCT volumes, aligning the images with the NHP.

- The method corrects misalignment in CBCT skull images due to involuntary head movements, ensuring accurate cephalometric measurements.
- Reference points like fronto-zygomatic sutures, ocular cavity centroids, and the Sella-Nasion line were used to adjust head position in all anatomical planes.
- The approach aligns CBCT volumes to the NHP after capture, reducing errors in cephalometric analysis and enhancing diagnostic accuracy.

☆ **Related research article:** None.
☆☆ ***For a published article:*** None.

* Corresponding author.
E-mail address: cferro@uao.edu.co (C.A.F. Sánchez).

https://doi.org/10.1016/j.mex.2024.103073
Received 19 August 2024; Accepted 25 November 2024
Available online 27 November 2024

Specifications table

Subject area:	Engineering
More specific subject area:	Health and Medical Sciences: Medical Imaging; Cephalometric Analysis; Craniofacial Morphology.
Name of your method:	Method for Correcting Natural Head Position in CBCT Volumes Using RAI Orientation, YOLOv8, and VGG19 (M-CNHP-RYV): A Sella-Nasion-Based Approach (SN-CM-NHP)
Name and reference of original method:	Key References: • **Lumbstrong Methodology for Sagittal Plane Correction:** ○ F. Lundström and A. Lundström, "Natural head position as a basis for cephalometric analysis," American Journal of Orthodontics and Dentofacial Orthopedics, vol. 101, no. 3, pp. 244–247, Mar. 1992, doi:10.1016/0889-5406(92)70093-p. • **VGG19-Based Technique for Cephalometric Point Detection:** ○ R. Chen, Y. Ma, N. Chen, D. Lee, and W. Wang, "Cephalometric Landmark Detection by Attentive Feature Pyramid Fusion and Regression-Voting," in Lecture notes in computer science, 2019, pp. 873–881. doi:10.1007/978-3-030-32248-9_97. This study trained a VGG19 network on lateral radiographs, adapted for sagittal projections from CBCT volumes.The corrections proposed in the axial and coronal planes, including the use of YOLOv8 for segmenting ocular cavities, are novel contributions developed specifically for this study and are not based on previously published methods.
Resource availability:	*None*

Background

The natural head position (NHP) is essential in cephalometric studies to obtain accurate measurements from lateral radiographic images, which are crucial in dental specialties such as orthodontics and maxillofacial surgery. Incorrect head orientation during image acquisition can distort parameters such as jaw length, anterior facial height, and mandibular body alignment [1–3]. This has a direct impact on the decisions made regarding the diagnosis and treatment of a patient [2,4,5]. Therefore, it is crucial to correct any misalignment caused by the patient's head rotation and tilt during image acquisition to minimize errors in cephalometric measurements, which are used to define appropriate treatment.

Cephalometric analyses that support specialists' decision-making are typically performed on lateral head radiographs, which only allow for correction in the sagittal plane. However, the use of CBCT images is becoming increasingly common, as they provide the specialist with more information for diagnosis and subsequent therapeutic decision-making. Additionally, these studies are becoming more accessible to patients [6]. Since CBCT scans contain volumetric information, they allow for the correction of the natural head position in all three anatomical planes (axial, coronal, and sagittal).

To mitigate potential errors in cephalometric measurements, two strategies have been addressed: one before acquisition [7] and others after acquisition [8,9]. The pre-acquisition strategies consist of protocols applied during the acquisition process. These protocols are implicit in the capture procedures, most of them using alignment laser guides that help ensure the head is in the correct position before acquisition. However, this does not guarantee that the patient will maintain the correct position during the capture. Therefore, it is possible that pre-acquisition methods may still require post-capture adjustment. In [7], the patient is first instructed on the required position in the sagittal and coronal planes, showing them their reflection in a mirror alongside the alignment laser projection of the equipment. Subsequently, the orientation of the Z-axis is adjusted by comparing the acquired images to a reference CBCT. In [8], the technique proposed in [4] was applied to 160 images, initially aligning the head in a reproducible position with the Frankfort horizontal plane parallel to the X-ray equipment, and finally adjusting the inclination of the plane between the Sella (S) and Nasion (N) points to 5.6° In [9] principal component analysis (PCA) was used to identify the orientations of the three axes, reorienting them to anatomical reference points in the naso-orbital region, this strategy was validated with 29 CBCT images. The present study proposes a post-capture strategy to correct the NHP in the anatomical planes, using stable anatomical references for the estimation of rotation angles, and was validated on 200 CBCT images [10].

Method details

Materials

In the present study, craniofacial images were acquired using two different cone beam computed tomography (CBCT) devices: the 17/19 model from Imaging Science International and the NNT/NTVGiMK4 model.

Methods

Despite the existence of protocols prior to taking a CBCT, the head position may differ from the desired one due to involuntary head movements by patients during acquisition, which can affect cephalometric measurements. Therefore, this study presents a methodology that allows for the correction of the natural head position in CBCT skull images by performing three processes: (1) standardization of the RAI orientation in the CBCT images, (2) estimation of rotation angles in the anatomical planes, and (3) correction of the CBCT volume to NHP.

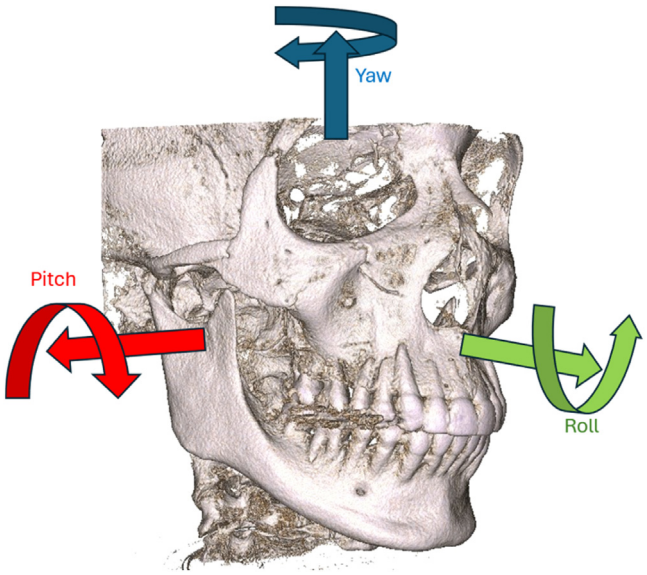

Fig. 1. Rotations in the three anatomical planes.

Each of these processes is described below:

1. **RAI orientation standardization in CBCT images**

The slices associated with the CBCT volume are often disordered, and if used in this state, they would result in an incorrect 3D volume reconstruction [1,11]. Although the "InstanceNumber" information is included in the metadata [12], it is often unreliable, requiring alternative sorting strategies. Additionally, CBCT images can use either the RAI (Right, Anterior, Inferior) or LPS (Left, Posterior, Superior) coordinate reference system, so it is necessary to normalize the volume orientation to one of the two. In this work, the RAI system was chosen because it is commonly used for radiographic image visualization and is simply the inverse of LPS.

The process begins by reorganizing the location of the slices, using the metadata information IOP (Image Orientation Patient) and IPP (Image Position Patient) [11], to estimate the slice's position index within the volume (Dp). The Dp is established by summing the projections of the orientation vector ($\overrightarrow{IPP}$) onto the normal vector ($\vec{n}$) of each slice [11]. In other words, the index corresponds to the value obtained from the dot product between these two vectors, as shown in Eq. (1).

$$Dp = \overrightarrow{n_X} \cdot \vec{IPP}_X + \overrightarrow{n_Y} \cdot \vec{IPP}_Y + \vec{1} \cdot \vec{IPP}_Z \tag{1}$$

Where the information from $\vec{IPP}_X$, $\vec{IPP}_Y$, e $\vec{IPP}_Z$ comes from the IPP metadata, while the normal vector ($\vec{n}$) is calculated according to Eq. (2).

$$\vec{n} = \vec{IOP}_X \times \vec{IOP}_Y \tag{2}$$

Where $\vec{IOP}_X$ is the vector corresponding to the column information contained in IOP_1 within the IOP metadata, and $\vec{IOP}_Y$ is the vector for the rows contained in IOP_2 within the IOP metadata.

The result of the previous process is that the slices will always be oriented in LPS, and to change them to RAI, it is sufficient to rotate all axes by 180° [13].

2. **Estimation of rotation angles in the anatomical planes**

The estimation of the Yaw rotation angle was performed in the axial plane, followed by the Roll angle in the coronal plane, and finally the Pitch angle in the sagittal plane. However, the NHP is not affected by the order in which these angles are estimated. Fig. 1 shows the direction of the mentioned rotations: Yaw (blue axis), Roll (green axis), and Pitch (red axis).

2.1. Estimation of the Yaw rotation angle

The analysis of the rotation angle in the axial plane (Yaw) requires the identification of two anatomical references with a low index of asymmetry or low variability between individuals. For this process, the two frontozygomatic sutures (FZS) were used as anatomical references due to their minimal variation between individuals, as well as their easy location and segmentation in the axial plane [14–16]. The Xs within the boxes in the left and right images in Fig. 2 correspond to an example of the location of the FZS.

To locate the FZS, the search is limited to slices containing information from the frontal process of the zygomatic bone to the zygomatic process of the frontal bone. Through a study of a subset of 100 images (half of the available ones), it was established that

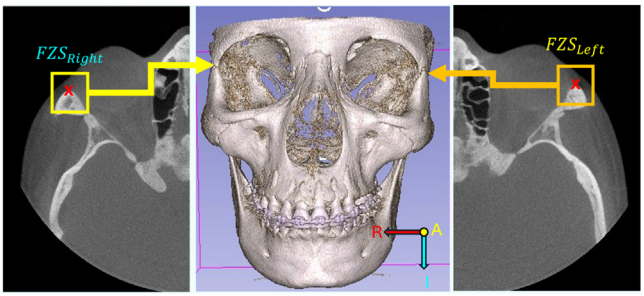

Fig. 2. Example of FZS location. Left - Right FZS located on the left half of the axial projection. Center - Reconstruction of the CBCT volume using the RAI reference system. Right - Left FZS located on the right half of the axial projection.

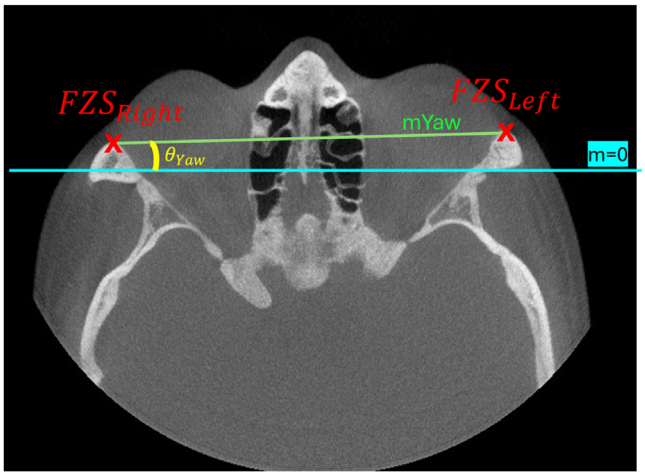

Fig. 3. Calculation of the Yaw angle in the axial MIP projection.

Tabla 1
Description of the subvolume location depending on the number of slices in the CBCT.

Volume size in cuts.	Location of the slices
≤= 350	290:310
≤= 450	350:370
≤= 510	370:390
≥= 540	450:490

it is sufficient to preserve a subvolume with 20 slices, whose location depends on the number of slices in the CBCT. Table 1 presents the location of the 20 slices according to the number of slices in the CBCT. The location is given in terms of the previously established slice position indices (Dp).

As shown in Fig. 3, the FZS corresponds to the pixels with maximum intensity at the edges of the axial projection. The axial projection corresponds to the maximum intensity projection (MIP) of the subvolume in the axial plane, which highlights the difference between bone and soft tissues. However, it is necessary to enhance the contrast of the MIPs due to differences in capture devices and their configurations, which vary by laboratory. To enhance contrast, the CLAHE (Contrast Limited Adaptive Histogram Equalization) algorithm [17–19] was used, ensuring that the output image histogram corresponds to a uniform distribution. The separation of the bone regions containing the FZS from the rest of the image (soft tissues and background) can be done automatically by defining a threshold based on the histogram of the contrast-enhanced image. The threshold corresponds to the mean value of the centroids of the two groups identified by the K-means clustering technique [20]. The coordinates of the right FZS ($FZS_{X-right}, FZS_{Y-right}$) will correspond to the minimum values of the X and Y coordinates in the bone region of the left half of the projection, while the coordinates of the left FZS ($FZS_{X-left}, FZS_{Y-left}$) correspond to the minimum value of the Y coordinates and the maximum value of the X coordinates.

Table 2
Hyperparameters and Increase parameters used that training Yolov8n seg.

Parameter	Value
Train epoch	70
Batch size	16
Learning rate	0.001
Momentum	0.937
Adjust image hue in a fraction (Hsv_h)	0.015
Alteration of image saturation in a fraction (Hsv_s)	0.7
Modify the brightness of the image in a fraction (Hsv_v)	0.4
Moving the image horizontally and vertically into a fraction of the image size (Translate)	0.1
Scaling the image to a given factor (Scale)	0.5
Turn the image left or right with a specified probability (Fliplr)	0.5

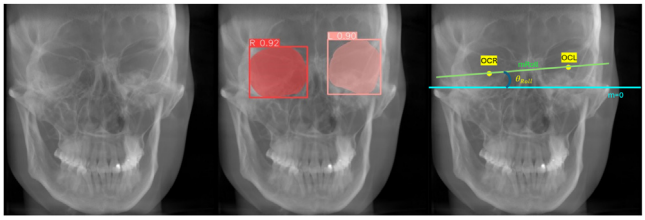

Fig. 4. Calculation of the roll angle in the coronal STDIP projection.

Fig. 3 shows how the Yaw rotation angle corresponds to the inclination angle of the slope of the line generated between the right and left reference points of the FZS (green line). This angle is obtained using Eq. (3).

$$\theta_{Yaw} = \operatorname{atan}\left(-\left(\frac{FZS_{Y_{left}} - FZS_{Y_{right}}}{FZS_{X_{left}} - FZS_{X_{right}}}\right)\right) \tag{3}$$

2.2. Estimation of the roll rotation angle

The estimation of the rotation angle in the coronal plane, known as Roll, provides detailed information about the lateral inclination of the head. To correct the NHP in this plane, the angle between the ocular cavities was calculated. Although several anatomical references with low variability can be used, in [15,16] mention that the ocular cavities are one of them, with the advantage of being a large area and having a marked difference between the tissues that compose them and the bony part, making them easily distinguishable. he location of the anatomical reference points of the ocular cavities corresponds to the centroid coordinates of the regions representing them: (OCR_X, OCR_Y) for the right ocular cavity, and (OCL_X, OCL_Y) p for the left one. To segment the ocular cavities from CBCT volumes, a deep learning model from the YOLO family, known for its good results in segmenting various objects [21,22], was used. Specifically, YOLOv8n-seg [23,24] was trained using 50 % of the available CBCT volume cases. Two projections were generated from each volume: the Maximum Intensity Projection (MIP), created from the subvolume containing information from the most anterior part of the face to the middle of the volume, and the Standard Deviation Projection (STDIP) extracted from the entire cranial CBCT volume [25]. Additionally, data augmentation was performed by applying random Roll rotations between −10° and 10° to these projections. The same data augmentation procedure was applied to the remaining user cases to test the segmentation performance of the model.

MIP images are obtained from the maximum intensity value of the coronal projection of the CBCT volume, while STDIP images correspond to the sum of the standard deviations of the coronal projection.

The ground truth for the segmentation of the ocular cavities corresponds to an irregular polygon generated using the Labelbox tool [26];thus, the model is provided with the coordinates of the vertices that compose the polygon as the desired output. Once trained, the model produces a binary image with the two regions associated with the ocular cavities. Table 2 contains the parameters used for training the model.

The Fig. 4 presents an example of estimating head inclination, given by the slope of the line connecting the anatomical references of the ocular cavities (green line). Left – STDIP projection, Center – result of the ocular cavity segmentation process by the model, Right – Estimated lateral inclination.

The correction angle in the coronal plane (θ_{Roll}) is given by the angle formed between the head's lateral inclination (green line in Fig. 4 right) and a horizontal line (blue line), as shown in Eq. (4).

$$\theta_{Roll} = \operatorname{atan}\left(-\left(\frac{OCL_Y - OCR_Y}{OCL_X - OCR_X}\right)\right) \tag{4}$$

Table 3
Training parameters Fusionvgg19.

Parameter	Value
Train epoch	150
Optimizer	Lion [29]
Batch size	1
Learning rate	0.0001
Weight decay	0.01
Dropout	0.3

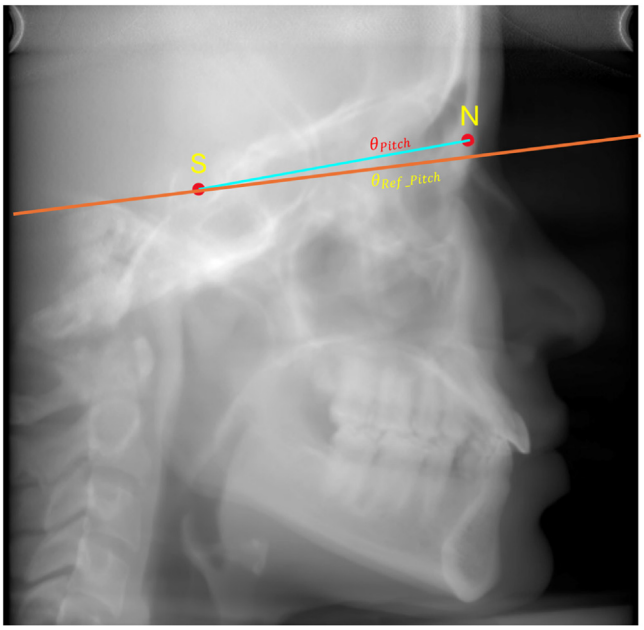

Fig. 5. Estimation of the Pitch rotation angle in sagittal SUMIP projection.

2.3. Estimation of the pitch rotation angle

The measurement of the rotation angle in the sagittal plane, known as Pitch, corresponds to the vertical inclination of the head (θ_{Pitch}). This angle is adjusted to a reference value $\theta_{Ref_{pitch}}$ of 3.8° for men and 4.1° for women, to correct the NHP in this plane [4]. To establish the vertical inclination in the CBCT volume, the anatomical reference is the line formed between the cephalometric points Sella (S) and Nasion (N). Although other anatomical references exist for estimating vertical inclination [9,27], the cephalometric points S and N are the most commonly used for this purpose due to their low variability [4,8].

The location of the anatomical reference points S (S_X, S_Y) and N (N_X, N_Y) is established using probability maps generated by a deep learning model based on the VGG-19 architecture, with modifications proposed by [28]. The model was trained with 300 images distributed as follows: 100 images of X-ray sum projection (SUMIP) and 100 of standard deviation projection (STDIP) from 100 patients (half of the available dataset), and another 100 randomly selected from the previous set of 200 images, with random Pitch rotations induced between −15° and 15°

The SUMIP and STDIP images are obtained as proposed in [25]. The SUMIP images correspond to the summation of voxel values in the direction of the sagittal plane, while the STDIP images correspond to the summation of the standard deviations of the sagittal projection, both derived from the CBCT volume. The ground truth for the anatomical references of S and N were manually defined by two clinical specialists in both types of images. Table 3 presents the parameters used in the model training process.

Fig. 5 presents the line formed between the anatomical references of S and N (blue line) and the vertical inclination required to correct the NHP in the sagittal plane (orange line). The posture correction angle (θ_{Pitch}) is the angle formed between these two lines, as shown in Eq. (5).

$$\theta_{Pitch} = \operatorname{atan}\left(-\left(\frac{N_Y - S_Y}{N_X - S_X}\right)\right) - \theta_{Ref_{pitch}} \tag{5}$$

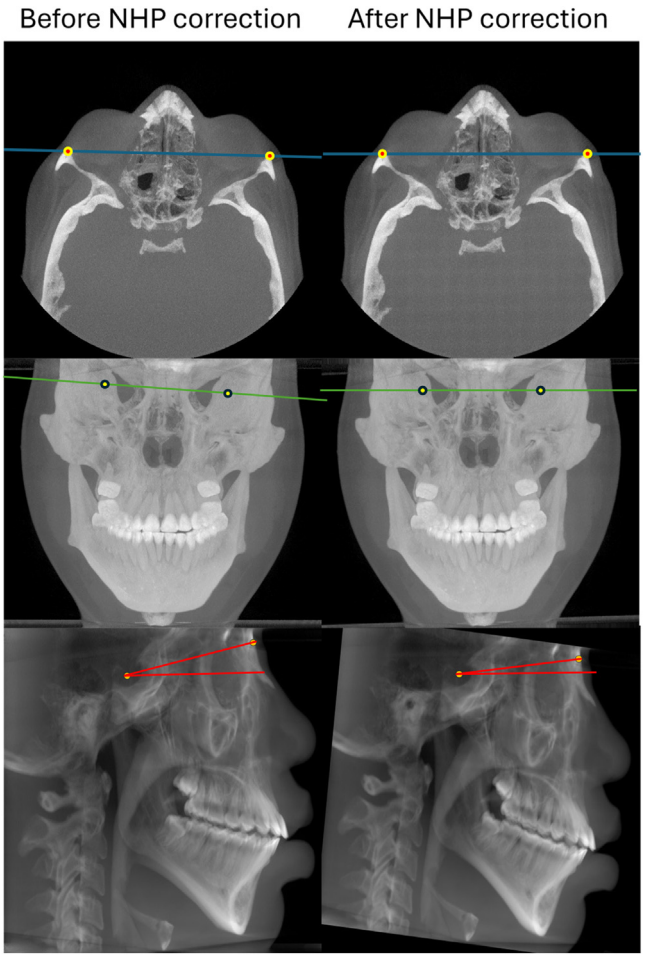

Fig. 6. NHP correction in the three anatomical planes (initial vs. with correction).

3. Correction of the CBCT volume to NHP

Once the rotation angles in the axial (θ_{Yaw}), coronal (θ_{Roll}), and sagittal (θ_{Pitch}), planes are established, the correction of the CBCT skull volumes is performed. Fig. 6 shows the initial volume projections in each plane on the left, and the corresponding corrected projections on the right.

Method validation

The validation process began with the calculation of the necessary sample size to ensure that the results would be representative, using a 95 % confidence level and a 5 % margin of error, as described in Eq. (6). Through this process, it was determined that the appropriate population for validating the methodology should consist of 132 subjects, ensuring that the sample is representative and that the results of the analysis are statistically significant.

$$n = \frac{\left(\frac{Z^2 \bullet p \bullet (1-p)}{e^2}\right)}{\left(1 + \left(\frac{Z^2 \bullet p \bullet (1-p)}{e^2 N}\right)\right)} \tag{6}$$

Where n is the sample size, Z is the statistical value for the desired 95 % confidence level (1.96), p is the estimated proportion of the characteristic of interest in the population (set at 0.5), e is the acceptable 5 % margin of error, and N is the population size (200).

The next step involved calibration with the two experts to ensure consistency and precision in the measurements. To achieve this, 20 images were randomly selected, equivalent to 10 % of the original sample, and used in a joint training session. This training process is crucial in validation studies to minimize inter-observer differences and ensure data reliability [30]. A practice session was conducted where the two investigators, referred to as Clinician 1 and Clinician 2, placed the anatomical references FZS right and left in both the axial and coronal planes, and the S and N points in the sagittal plane, on the same images. The results were then discussed. A tolerance of 0.5° was established for the measurement of angles, and Cohen's Kappa coefficient [31] was calculated

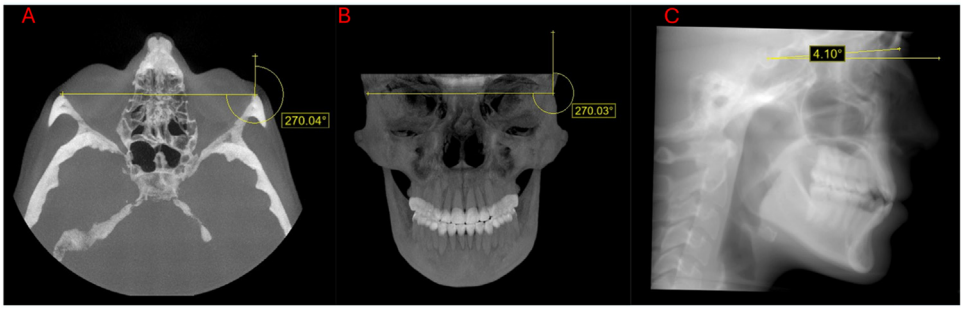

Fig. 7. Validation of subject CoF traced by one of the clinicians: A. Axial view, B. Coronal view, C. Sagittal view.

using Eq. (7), resulting in a 95 % agreement between the measurements of the two clinicians. This ensured consistency and proper calibration before proceeding with the validation in the main sample.

$$K = \frac{p_0 - p_e}{1 - p_e} \tag{7}$$

Once the concordance evaluation was completed, 132 subjects were selected from the population of 200 cases through a random permutation process [32]. This method ensures an equitable and representative selection of the sample, minimizing potential biases in the composition of the validation group.

An individual table was created for each clinical professional. In the first column, labeled "image," the randomly selected subjects were recorded. The second column contained the data collected by the clinician in the axial view, while the third column was designated for the coronal view, and the fourth column for the sagittal view. It is important to note that each clinician worked independently, without access to the other's information.

Using BlueSky Plan software version 4.13.31, each clinician obtained validation data through the cephalometric analysis module. The images, automatically corrected for head position, were analyzed in the axial, coronal, and sagittal planes using angular measurement tools. The measurement process in each plane was carried out as follows:

1. To validate the axial position, the clinicians measured the angle formed by the slope between the FZS right and FZS left points, which correspond to the pixels of maximum intensity at the extremes of the axial projection, as shown in Fig. 7A. From the FZS left, a second vertical line was drawn upward, forming an angle with the previously traced slope between the FZS points. The resulting angle was measured, and 270° was subtracted from this value to normalize the measurement with respect to a standard reference. The resulting value was recorded in the validation table under the axial column.
2. The validation of the coronal projection involved measuring the angle formed between the outermost regions of the fronto-zygomatic suture, or the fronto-maxillary suture, and a true vertical line or vertical line drawn upward, as shown in Fig. 7B. This resulting angle was reduced by 270°, and the obtained value was recorded in the validation table under the coronal column.
3. The validation of the correction in the sagittal plane involved measuring the internal angle formed between the S and N points and a zero-slope line passing through point S, as shown in Fig. 7C. The results were recorded in the validation table under the sagittal column.

In the analysis of the validation of the proposed methodology for the correction of the natural head position (NHP) across the three anatomical planes, angular measurements performed by clinicians on corrected images were utilized and analyzed using various error metrics to determine the precision and reliability of the implemented technique.

In the sagittal plane, the root mean squared error (RMSE) was 0.029° for women and 0.032° for men, with standard deviations of ±0.021° and ±0.027°, respectively. In the axial plane, the RMSE was 0.0189° for women and 0.0377° for men, with corresponding standard deviations of ±0.0174° and ±0.0261° Similarly, in the coronal plane, the RMSE was 0.0240° for women and 0.0238° for men, with standard deviations of ±0.0218° and ±0.0188° These errors are notably lower than those reported in other methodologies and are minimal, suggesting a potential influence of human error [33–35]. Furthermore, a Bland-Altman analysis [30] demonstrated strong agreement between the two clinicians' measurements, with most differences falling within pre-established limits and no indication of systematic bias.

Limitations

Although the methodology has proven to be effective in correcting the natural head position (NHP) in CBCT images using stable anatomical references, several limitations must be considered:

1. **Absence of a universal ground truth:**
   The natural variability of head position among individuals and ethnic groups makes it impossible to create a single ground truth that can be applied to the entire population without introducing inaccuracies. The NHP varies between patients due to anatomical and functional factors, which makes a standardized ground truth unsuitable for all individuals. This has been corroborated in

studies showing that cephalometric positioning and references such as the Sella-Nasion line and the Frankfort plane exhibit significant variations between different ethnic groups and even within the same groups [36–41]. Therefore, the use of a synthetic ground truth could compromise clinical accuracy and generate false positives.

2. **Expert calibration and scalability:**
   It is recognized that expert calibration is an effective method for ensuring the accuracy of cephalometric measurements. However, this process requires significant resources and is not easily scalable to large volumes of data. Despite this, our validation approach has proven reliable in studies that have used stable anatomical references for corrections in the axial, coronal, and sagittal planes [8,9,14,16]. In future studies, we plan to explore automated methods for the identification of cephalometric points to make the validation process more efficient without compromising the precision of the methodology.
3. **Anatomical variability:**
   The anatomical landmarks used in the methodology, such as Sella and Nasion, as well as the frontozygomatic suture in the axial plane and the centroid of the orbital cavity in the coronal plane, are known to vary among individuals and different ethnic groups. However, these structures exhibit variability within permissible ranges, allowing them to be considered stable references in clinical contexts [14,16,27]. Previous studies have demonstrated that both the Sella-Nasion line and the Frankfort horizontal plane show significant differences between populations, reinforcing our decision to use patient-specific anatomical references rather than a standardized ground truth [40,42–44].
4. **Applicability in diverse populations:**
   Although the study focused on a mestizo population, additional research in populations with different craniofacial characteristics is necessary to evaluate the generalization of the results. Previous studies have shown that structures such as the orbital cavity and zygomatic sutures vary significantly between populations, which can influence the accuracy of the applied corrections [14,40,42,43]. This suggests the need for broader studies that address population diversity to improve the applicability of our methodology in various clinical settings.

Ethics statements

During the data collection of this study, strict ethical considerations were followed:

- Patients' consent was obtained prior to the acquisition of the images, and no personal information was included in the records.
- To ensure patient anonymity, all personally identifiable information was removed from the images.
- Additionally, the study was approved by the Ethics Committee of the Universidad Autónoma de Occidente under ETHICS COMMITTEE ACT No. 01–2024 of February 12, 2024, thereby ensuring compliance with current ethical standards in medical research.
- The collection of these images was conducted in accordance with the Declaration of Helsinki issued by the World Medical Association.

Credit author statement

Carlos Andrés Ferro Sanchez*:* Conceptualization, Methodology, Software, Investigation, Writing - Original Draft, Visualization, Supervision; **Cristian Orlando Diaz Laverde:** Methodology, Validation, Investigation, Writing - Original Draft; **Sandra Esperanza Nope Rodríguez:** Software, Methodology, Writing - Review & Editing; **Gilbert Alexis Corrales Gallego**: Software, Writing, Methodology; **Juan Fernando Aristizábal:** Validation; **Oscar Iván Campo Salazar:** Writing - Original Draft.

Declaration of competing interest

The authors declare that they have no known competing financial interests or personal relationships that could have appeared to influence the work reported in this paper.

Data availability

The data that has been used is confidential.

Acknowledgments

This research did not receive any specific grant from funding agencies in the public, commercial, or not-for-profit sectors.

References

[1] S. Nowak, A.M. Sprinkart, Synchronization and alignment of follow-up examinations: a practical and educational approach using the DICOM reference coordinate system, J. Digit. Imaging 32 (1) (Aug. 2018) 68–74 *2018 32:1*, doi:10.1007/S10278-018-0117-4.

[2] S. Malkoc, Z. Sari, S. Usumez, A.E. Koyuturk, The effect of head rotation on cephalometric radiographs, Eur. J. Orthod. 27 (2005) 315–321, doi:10.1093/ejo/cjh098.

[3] A. Shokri, A. Miresmaeili, N. Farhadian, S. Falah-Kooshki, P. Amini, N. Mollaie, effect of changing the head position on accuracy of transverse measurements of the maxillofacial region made on cone beam computed tomography and conventional posterior-anterior cephalograms, Dentomaxillofac. Radiol. 46 (2017), doi:10.1259/dmfr.20160180.

[4] F. Lundström, A. Lundström, Natural head position as a basis for cephalometric analysis, Am. J. Orthod. Dentofac. Orthoped. 101 (3) (Mar. 1992) 244–247, doi:10.1016/0889-5406(92)70093-P.

[5] D.M. Ramírez, J. Canseco Jiménez, E. González Ramírez, H. Jaramillo Paniagua, V. Cuairán Ruidíaz, Discrepancies in cephalometric measurements in relation to natural head position, Rev. Mex. Ortodoncia 1 (1) (Oct. 2013) e27–e32, doi:10.1016/S2395-9215(16)30117-9.

[6] K. Işınlı, B. Tomografinin, T. Kavramları, D. Kullanım, A.E. Venkatesh, and S.V. Elluru, "Cone beam computed tomography: basics and applications in dentistry", doi:10.17096/jiufd.00289.

[7] T.C. Hsung, W.K. Yeung, W.S. Choi, W.K. Luk, Y.Y. Cheng, Y.H. Lam, Recording natural head position using cone beam computerized tomography, Sensors (Basel) 21 (24) (Dec. 2021), doi:10.3390/S21248189.

[8] A. Alhumadi, T.J. Al-Khafaji, A.M.H. Alyassiri, W.W. Alhamadi, Gender differences in lower facial soft tissue thickness among different skeletal patterns, based on soft tissue cephalometric analysis, J. Orthod. Sci. 11 (1) (Oct. 2022), doi:10.4103/JOS.JOS_38_22.

[9] U. Mangal, et al., Reorientation methodology for reproducible head posture in serial cone beam computed tomography images, Sci. Rep. 13 (1) (Dec. 2023) 3220, doi:10.1038/S41598-023-30430-4.

[10] C.A.F. Sánchez, C.O.D. Laverde, S.E.N. Rodríguez, J.F. Aristizábal, O.I.C. Salazar, Sagittal cranial projections dataset extracted from CBCT volumes corrected to natural head position in a mixed ethnicity population, Data Brief. (Jun. 2024) 110622, doi:10.1016/J.DIB.2024.110622.

[11] D. Atkinson, "Geometry in medical imaging: DICOM and NIfTI formats," 2022.

[12] "Digital Imaging and Communications in Medicine (DICOM) Part 3: Information Object Definitions," 2011.

[13] G.L. Kindlmann, "An self-contained explanation of image orientation and the 'measurement frame', with connections to the NRRD format (Version 0.5)," 2010, Accessed: Jun. 02, 2024. [Online]. Available: http://www.na-mic.org/Wiki/index.php/NAMIC_Wiki:DTI:Nrrd_format.

[14] D.C.O. Coutinho, P.A. Martins, I. Campos, A.L.N. Custódio, M.R.M. Alves E Silva, Zygomaticofacial, zygomaticoorbital, and zygomaticotemporal foramina, J. Craniofac. Surg. 29 (6) (2018) 1583–1587, doi:10.1097/SCS.0000000000004530.

[15] R. Tandon, L. Aljadeff, S. Ji, R.A. Finn, Anatomic variability of the human orbit, J. Oral Maxillofac. Surg. 78 (5) (May 2020) 782–796, doi:10.1016/J.JOMS.2019.11.032.

[16] F. Seiji, R.S. Moreira, M.A. De Angelis, R.L. Smith Chairman, Orbital asymmetry in development: an anatomical study, Orbit. 28 (6) (Dec. 2009) 342–346, doi:10.3109/01676830903162841.

[17] S. Rahman, M.M. Rahman, M. Abdullah-Al-Wadud, G.D. Al-Quaderi, M. Shoyaib, An adaptive gamma correction for image enhancement, EURASIP J. Image Video Process. 2016 (1) (Dec. 2016), doi:10.1186/S13640-016-0138-1.

[18] Y. Yoshimi et al., "Image preprocessing with contrast-limited adaptive histogram equalization improves the segmentation performance of deep learning for the articular disk of the temporomandibular joint on magnetic resonance images," *Oral Surg. Oral Med. Oral Pathol. Oral Radiol.*, Apr. 2023, doi:10.1016/J.OOOO.2023.01.016.

[19] Y. Zhou, C. Shi, B. Lai, G. Jimenez, Contrast enhancement of medical images using a new version of the world cup optimization algorithm, Quant. ImAging Med. Surg. 9 (9) (2019) 1528, doi:10.21037/QIMS.2019.08.19.

[20] M.R. Collier, et al., A K-means clustering analysis of the jovian and terrestrial magnetopauses: a technique to classify global magnetospheric behavior, J. Geophys. Res. Planets. 125 (9) (Sep. 2020) e2019JE006366, doi:10.1029/2019JE006366.

[21] M. Automated et al., "Citation: automated left ventricle segmentation in echocardiography using YOLO: a deep learning approach for enhanced cardiac function assessment," 2024, doi:10.3390/electronics13132587.

[22] X. Yue, K. Qi, X. Na, Y. Zhang, Y. Liu, and C. Liu, "Improved YOLOv8-Seg network for instance segmentation of healthy and diseased tomato plants in the growth stage," 2023, doi:10.3390/agriculture13081643.

[23] G. Jocher, A. Chaurasia, J. Qiu, Ultralytics YOLO, *Ultralytics*: 8.0.0 (2013). https://github.com/ultralytics/ultralytics.

[24] X. Jiang, X. Zhuang, J. Chen, J. Zhang, Y. Zhang, YOLOv8-MU: an improved YOLOv8 underwater detector based on a large kernel block and a multi-branch reparameterization module, Sensors. (Basel) 24 (9) (May 2024), doi:10.3390/S24092905.

[25] M. Prokop, M. Galanski, A.J. Van Der Molen, and C. Schaefer-Prokop, *Spiral and multislice computed tomography of the body*. 2001.

[26] "Labelbox | Data factory for the next GenAI." Accessed: Aug. 13, 2024. [Online]. Available: https://labelbox.com/

[27] A. Lundström, F. Lundström, L.M.L. Lebret, C.F.A. Moorrees, Natural head position and natural head orientation: basic considerations in cephalometric analysis and research, Eur. J. Orthod. 17 (2) (Apr. 1995) 111–120, doi:10.1093/EJO/17.2.111.

[28] R. Chen, Y. Ma, N. Chen, D. Lee, and W. Wang, "Cephalometric landmark detection by attentive feature pyramid fusion and regression-voting".

[29] X. Chen et al., "Symbolic discovery of optimization algorithms," Feb. 2023, Accessed: Jun. 09, 2024. [Online]. Available: https://arxiv.org/abs/2302.06675v4

[30] D.S. Warner, J.M. Bland, D.G. Altman, Classic papers revisited agreed statistics measurement method comparison identifying a problem, Anesthesiology 116 (1) (2012) 182–187 Accessed: Aug. 07, 2024. [Online]. Available: http://pubs.asahq.org/anesthesiology/article-pdf/116/1/182/256631/0000542-201201000-00030.pdf .

[31] J.L. Cerda and L.P. Villarroel Del, "Evaluación de la concordancia inter-observador en investigación pediátrica: Coeficiente de Kappa".

[32] P. Bickel, P. Diggle, S. Fienberg, U. Gather, I. Olkin, and S. Zeger, "Springer series in statistics".

[33] A. Hróbjartsson et al., "Observer bias in randomized clinical trials with measurement scale outcomes: a systematic review of trials with both blinded and nonblinded assessors," 2013, doi:10.1503/cmaj.120744.

[34] P. Brennan and A. Silman, "Education & Debate statistical methods for assessing observer variability in clinical measures".

[35] L. Quinn, et al., Interobserver variability studies in diagnostic imaging: a methodological systematic review, Br. J. Radiol. 96 (1148) (Aug. 2023), doi:10.1259/BJR.20220972/SUPPL_FILE/SUPPLEMENTARY.

[36] M. Ijaz, E. Amin, N. Adnan, K. Ijaz, Comparison of Sella-Nasion to frankfort-horizontal plane angle between genders in different sagittal classes of malocclusion, Pak. Orthodont. J. 13 (1) (Jul. 2021) 25–30 Accessed: Oct. 14, 2024. [Online]. Available: https://www.poj.org.pk/index.php/poj/article/view/305 .

[37] R. Taylor and E. Schneiderman, "Exploring the sources of variation in the SN-FH angle and its components: a comparison of three ethnic groups," Apr. 16, 2021. Accessed: Oct. 14, 2024. [Online]. Available: https://hdl.handle.net/1969.1/195727.

[38] U. Mangal, et al., Effects of Changes in the Frankfort horizontal plane definition on the three-dimensional cephalometric evaluation of symmetry, Appl. Sci. 10 (22) (Nov. 2020) 7956 *2020, Vol. 10, Page 7956*, doi:10.3390/APP10227956.

[39] L.G. Farkas, et al., International anthropometric study of facial morphology in various ethnic groups/races, J. Craniofac. Surg. 16 (4) (Sep. 2005) 615–646, doi:10.1097/01.SCS.0000171847.58031.9E.

[40] H. Khani, Z. Fazelinejad, M.G. Hanafi, A. Mahdianrad, A.R. Eftekhari Moghadam, Morphometric and volumetric evaluations of orbit using three-dimensional computed tomography in southwestern Iranian population, Transl. Res. Anatomy 30 (Mar. 2023) 100233, doi:10.1016/J.TRIA.2023.100233.

[41] T. Khaitan, Vishal, P. Gupta, S.R. Naik, A.K. Shukla, Morphometric analysis of Sella Turcica and a proposed Novel Sella Turcica index – A digital lateral cephalometric study, Indian J. Otolaryngol. Head Neck Surg. 76 (1) (Feb. 2024) 73–77, doi:10.1007/S12070-023-04082-9/FIGURES/2.

[42] A. Franke, E.C. Hofmann, A. Steinberg, G. Lauer, H. Kitzler, H. Leonhardt, Probing real-world central European population midfacial skeleton symmetry for maxillofacial surgery, Clin. Oral. Investig. 27 (9) (Sep. 2023) 5637–5647, doi:10.1007/S00784-023-05185-X.

[43] V.K. Vaidya, S. Saha, P.S. Aneja, N. Kapur, S.K. Rathi, Morphometry of Sella Turcica, anterior clinoid process and carotico-clinoid foramen among North Indian population: a cross-sectional study, J. Clin. Diagn. Res. (2022), doi:10.7860/JCDR/2022/58224.16889.

[44] G.K. Shrestha, P.R. Pokharel, R. Gyawali, B. Bhattarai, J. Giri, The morphology and bridging of the sella turcica in adult orthodontic patients, BMC. Oral Health 18 (1) (Mar. 2018) 1–8 *2018 18:1*, doi:10.1186/S12903-018-0499-1.